Downloaded from orbit.dtu.dk on: May 05, 2023

DTU Library

Experimental and numerical validation of active flaps for wind turbine blades

Gomez Gonzalez, A; Enevoldsen, P B; Akay, B; Barlas, T K; Fischer, Andreas; Aa Madsen, H

Published in:
Journal of Physics: Conference Series

Link to article, DOI:
10.1088/1742-6596/1037/2/022039

Publication date:
2018

Document Version
Publisher's PDF, also known as Version of record

Link back to DTU Orbit

Citation (APA):
Gomez Gonzalez, A., Enevoldsen, P. B., Akay, B., Barlas, T. K., Fischer, A., & Aa Madsen, H. (2018). Experimental and numerical validation of active flaps for wind turbine blades. *Journal of Physics: Conference Series*, *1037*(2), [022039]. https://doi.org/10.1088/1742-6596/1037/2/022039

General rights
Copyright and moral rights for the publications made accessible in the public portal are retained by the authors and/or other copyright owners and it is a condition of accessing publications that users recognise and abide by the legal requirements associated with these rights.

- Users may download and print one copy of any publication from the public portal for the purpose of private study or research.
- You may not further distribute the material or use it for any profit-making activity or commercial gain
- You may freely distribute the URL identifying the publication in the public portal

If you believe that this document breaches copyright please contact us providing details, and we will remove access to the work immediately and investigate your claim.

Journal of Physics: Conference Series

PAPER • OPEN ACCESS

Experimental and numerical validation of active flaps for wind turbine blades

To cite this article: A Gomez Gonzalez *et al* 2018 *J. Phys.: Conf. Ser.* **1037** 022039

View the article online for updates and enhancements.

Related content

- Benchmarking aerodynamic prediction of unsteady rotor aerodynamics of active flaps on wind turbine blades using ranging fidelity tools
  Thanasis Barlas, Eva Jost, Georg Pirrung et al.
- Finite Element Analysis for the Web Offset of Wind Turbine Blade
  Bo Zhou, Xin Wang, Changwei Zheng et al.
- Wireless Sensors for Wind Turbine Blades Monitoring
  N Iftimie, R Steigmann, N A Danila et al.

IOP ebooks™

Bringing you innovative digital publishing with leading voices to create your essential collection of books in STEM research.

Start exploring the collection - download the first chapter of every title for free.

This content was downloaded from IP address 192.38.67.116 on 29/06/2018 at 10:11

IOP Conf. Series: Journal of Physics: Conf. Series **1037** (2018) 022039 doi:10.1088/1742-6596/1037/2/022039

Experimental and numerical validation of active flaps for wind turbine blades

A Gomez Gonzalez[1], P B Enevoldsen[1], B Akay[1], T K Barlas[2], A Fischer[2], H Aa Madsen[2]

[1]Siemens Gamesa Renewable Energy A/S, Brande, DK
[2]DTU Dept. of wind eneregy, Roskilde, DK

E-mail: alejandro.gonzalez@siemens.com

Abstract.

An industrial active flap concept for wind turbine rotor blades is validated numerically by means of CFD, as well as experimentally in a wind tunnel environment. This paper presents the numerical and experimental results, as well as a discussion regarding the testing of airfoils equipped with active flaps with a highly loaded aft portion. A conceptual implementation for an offshore wind turbine and the potential for load reduction is shown by means of aeroelastic calculations. The work presented herein is conducted within the frame of the Induflap2 project and is partially funded by the Danish funding board EUDP.

1. Introduction

An active flap system (AFS) is designed with the goal of industrial application on large (multi-megawatt) wind turbine blades. For this purpose, the AFS is designed for external mounting (add-on concept) on an existing blade, and the activation is performed via a pneumatic system. For testing purposes, two prototypes are manufactured with different materials: TPU (Thermoplastic Polyurethane) and silicone. The main difference between the two prototypes is the stiffness response of the full system, and thus the aerodynamic sensitivity measured in terms of lift variation as a function of pneumatic pressure. Prior to the simulation and testing of the active flap prototypes, a series of static flap variations are tested in order to validate the design methods. Finally, the load alleviation potential for such an active flap system is discussed. The work presented in this paper is part of the Induflap2 project [1], funded partially by EUDP [5], with the goal of demonstrating the potential of an active flap system via full-scale implementation. Within the project, a full palette of analysis and testing methods is used, including CFD, FEM, FSI, and aeroelastic simulations, together with testing at wind tunnel, rotating rig, and full-scale turbine level.

2. Validation of static flap configuration

Before testing the AFS, three different static flap configurations (see figure 1) are tested numerically and experimentally in order to assess the levels of variation of the aerodynamic characteristics (lift, drag, and moment coefficients) and to validate the numerical simulations. The static flap configurations consisted of three different deflection states of a slender flap (neutral, positive, and negative deflection). The purpose of testing and simulating these flaps is


Content from this work may be used under the terms of the Creative Commons Attribution 3.0 licence. Any further distribution of this work must maintain attribution to the author(s) and the title of the work, journal citation and DOI.
Published under licence by IOP Publishing Ltd

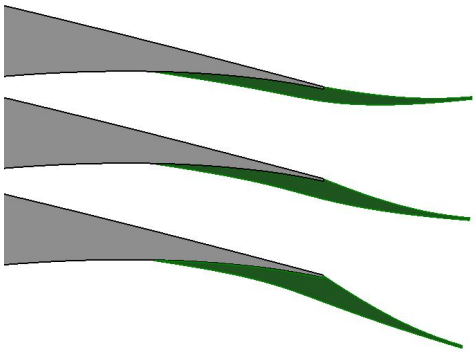

Figure 1: Static flap configurations. Upper: negative flap deflection (approx. -8 deg), middle: neutral flap deflection, lower: positive flap deflection (approx. 8 deg)

mainly to assess the level of predictability of lift variations of airfoils with heavy aft loading via CFD.

The CFD simulations are performed with two different codes, EllipSys [7, 8, 9] and Ansys CFX v15 [6] for a Reynolds number of 4 million. The simulations performed with EllipSys are based on a SST k-ω turbulence model [16] coupled with a e^N transition model with $N = 9$. These are performed on an O-mesh grid (see figure 2). The grid consists of 512 cells along the aerofoil surface and 192 in normal direction. The domain size in the direction normal to the surface is 40 chord lengths and the height of the cell on the aerofoil surface is 10^{-7} chord lengths. The stretching of the cells in normal direction is steered by an hyperbolic tangent function. The simulations performed with Ansys CFX r15 are based on a SST k-ω turbulence model coupled with a $Re_\theta - \gamma$ transition model, with a computational domain of approx. 235,000 elements. An example of the mesh resolution around the trailing edge of the airfoil-flap arrangement for both Ansys CFX and EllipSys is shown in figure 2.

Good agreement between both codes (and experiments as will be discussed further below) is found for the linear range of the lift curve for the cases of neutral flap deflection, i.e. without a flap deflection angle. On the contrary, it is shown that for the cases of positive and negative flap deflections, CFD results slightly overestimate the range of lift variation when compared to wind tunnel measurements based on pressure taps as shown in the two upper plots of figure 3. A difference between both codes is seen in the prediction of the stall AoA, where EllipSys has a tendency to overpredict the stall level.

The experimental wind tunnel validation of both the static flap configurations as well as of the AFS is performed at the Low Speed Low Turbulence wind tunnel facilities of the faculty of aerospace of TU Delft. For all flap configurations (both static and active), the lift coefficient is estimated simultaneously via pressure taps measurements directly on the airfoil surface, as well as via pressure measurements on the walls of the wind tunnel. The flaps themselves are not instrumented with pressure taps due to the technical complexity related to this. As mentioned, (see upper plots of figure 3), the estimation of aerodynamic coefficients via pressure taps on the airfoil model underestimates the lift variation levels as predicted by CFD. The reason for this is shown to be the strong local pressure gradients on the flap itself. Due to the nature of the flap (being an add-on, and not a morphing trailing edge), the local curvature is high in comparison with the curvature of the original airfoil.

Contrary to a morphing trailing edge, where the pressure distribution on the aft portion of the airfoil is small, an add-on AFS of this type causes strong localized pressure gradients in the

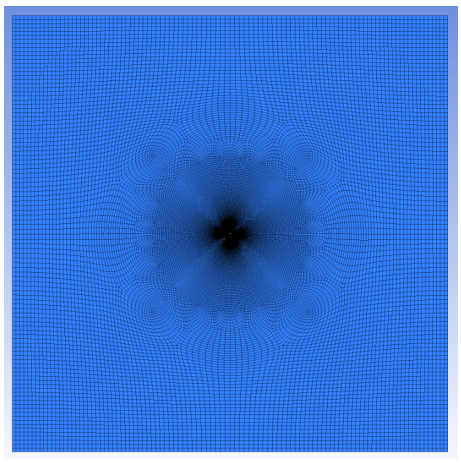

(a) Full domain grid for Ansys CFX simulations

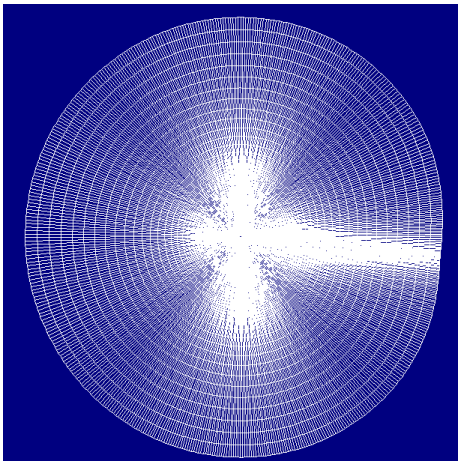

(b) Full domain grid for EllipSys simulations

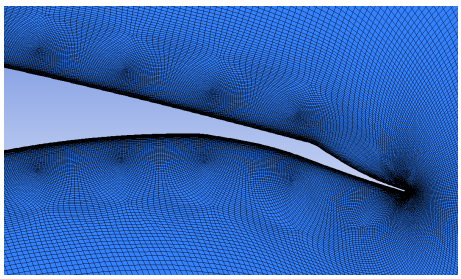

(c) Example for Ansys CFX simulations (neutral deflection)

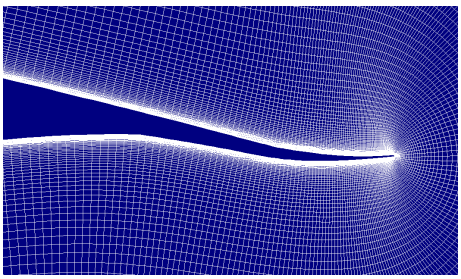

(d) Example for EllipSys simulations (negative deflection)

Figure 2: Computational grid comparison

trailing edge area due to the high curvature of the surface. In extreme flap deflection cases, the risk of localized flow separation also exists. Figure 4 depicts the non-dimensional pressure distribution of the different flap configurations for two particular angles of attack, namely $4deg$ and $8.5deg$). There is general good agreement between measurements and simulations. A slight discrepancy is seen at the higher AoAs with respect to the suction peak close to the leading edge of the airfoil. This is believed to be due to a manufacturing deviation of the wind tunnel model.

Special attention should be paid to the pressure distribution close to the trailing edge. Due to the absence of pressure taps on the AFS, the direct estimation of lift coefficients via pressure measurements includes the uncertainty of the c_p distribution around the trailing edge of the airfoil-flap arrangement. It can be seen from figure 4 that for a neutral deflection (middle plots), the error incurred when omitting the pressure distribution in the aft portion of the airfoil is small. In contrast, for both positive and negative flap deflections, the area contained between the Cp curves (related to the lift contribution in this area) is not negligible. For negative flap deflections (i.e. towards the suction side), the local curvature of the flap arrangement leads even to an inversion of the pressure distribution generating local suction pointing downwards on the pressure side of the flap. These high local pressure gradients are captured correctly in CFD, but not in the wind tunnel setup as shown in figure 4.

To overcome this difficulty, the lift coefficient measured with the pressure on the walls of

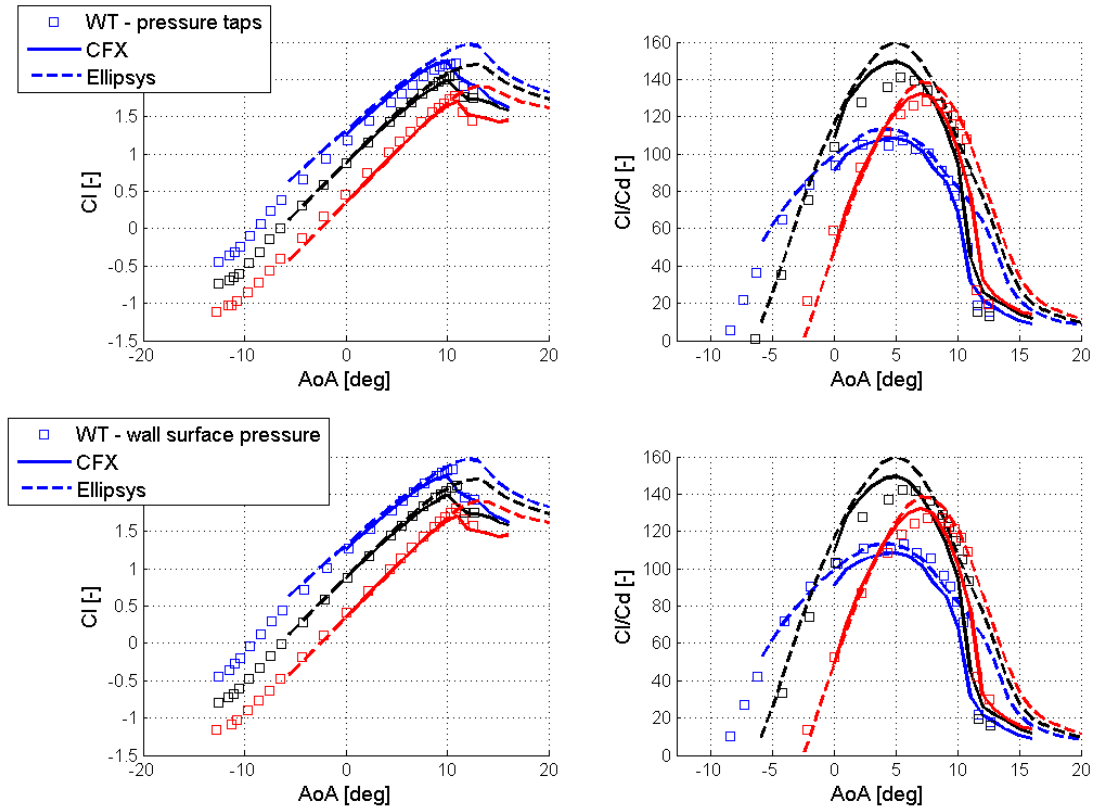

Figure 3: Comparison of lift coefficient (left plots) and lift to drag ratio (right plots) between simulations and experiments for a Reynolds number of 4 million. Top plots: measurements based on pressure taps, bottom plots: measurements based on wall surface pressure. Blue: +8 deg flap deflection, black: 0 deg flap deflection, red: -8 deg flap deflection.

the wind tunnel is used in order to validate the CFD calculations. The comparison of the measurements based on wall pressure and CFD simulations is shown in the bottom two plots of figure 3, showing a much better agreement. It is believed that the best approach for estimating the lift forces on an airfoil with an add-on active flap is via tunnel wall pressure measurement. To obtain the pressure distribution on the airfoil-flap arrangement, the direct pressure measurement on the airfoil is blended with the pressure distribution of the trailing edge area as obtained from CFD. The drag coefficients are obtained via measurement of the momentum deficit with a wake rake traversed to cover a representative extension of the model's span, which is accurate enough.

3. Validation of active flap configuration

The active flap system (AFS) has been tested for prototypes manufactured with two different materials of varying stiffness. The first material tested is a thermoplastic polyurethane (TPU), which is a type of thermoplastic elastomere well suited for extrusion purposes. The TPU grade used for this first wind tunnel prototype can be modelled as an isotropic material with hardness Shore 80A. The second prototype is manufactured using silicone with hardness Shore 60A. Even though there are several differences in terms of mechanical properties between these two materials, the focus of the current evaluation is placed on the stiffness response of the flap (i.e. ignoring for the moment other properties such as temperature dependence of stiffness,

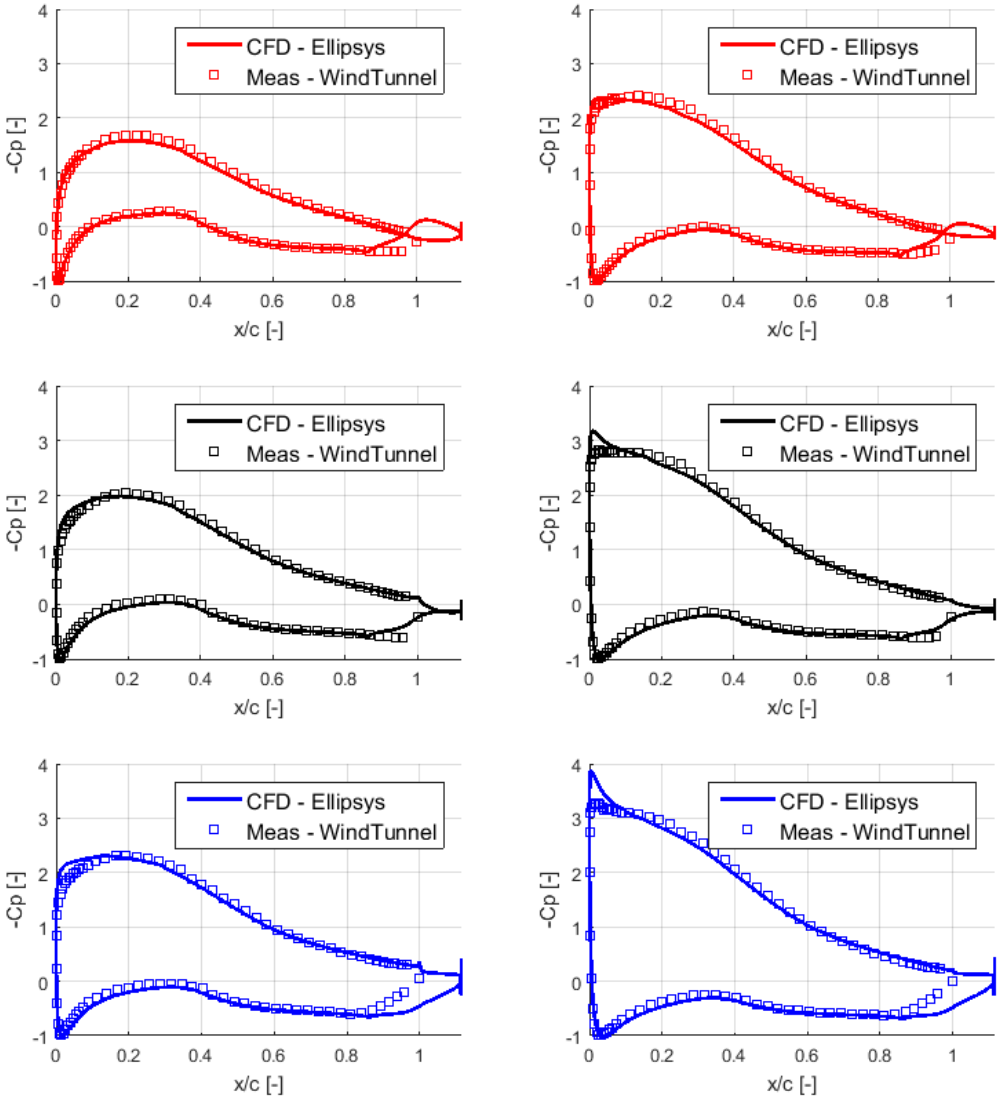

Figure 4: Exemplary comparison of pressure distributions of static flap configurations at 4 deg (left plots) and 8.5 deg (right plots). Upper: negative flap deflection (approx. -8 deg flap deflection). Middle: neutral flap deflection. Lower: positive flap deflection (approx. 8 deg flap deflection)

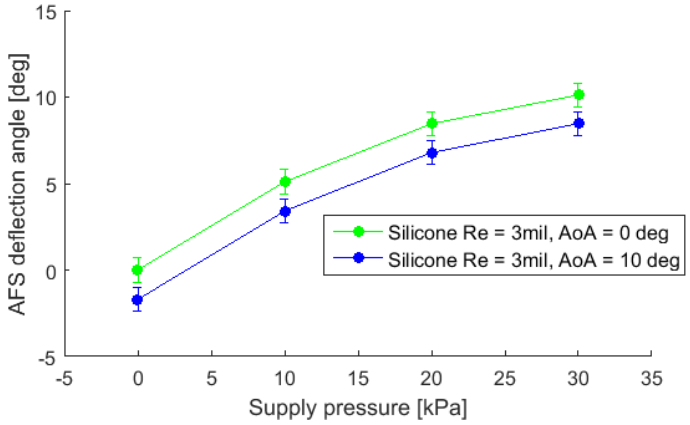

Figure 5: Deflection of silicone AFS as a function of actuation pressure input

brittleness, fatigue properties, etc).

The AFS is activated via pneumatic pressure supplied externally through the wind tunnel walls. The aerodynamic response of the full system is tested for a range of Reynolds numbers between 1 and 3 million, and for pressure supply levels varying between 0 and 50 kPa.

As a first step, the two AFS are characterized in terms of deflection response as a function of input pressure. The deflection is measured relative to the undeformed position at a charachteristic location on the flap approx. 85mm behind the trailing edge of the model (which has a chord of 900mm). The elastic response of the TPU prototype showed up to be highly mechanically restrained leading to a limited aerodynamic response with respect to flap actuation. For a full range pressure supply of 50 kPa, the TPU flap deflection lead to a change in lift coefficient (at AoA = 6 deg) of approx. 0.1, rendering this design not well suited for the purpose of the AFS, and will therefore not be further dealt with within the scope of this paper.

The deflection response of the silicone prototype is shown in figure 5 for a Reynolds number of 3 million and for AoA of 0 and 10 deg, respectively. The elastic response for both angles of attack is initially linear at low actuation pressures, and starts becoming non-linear for actuation pressures approx. larger than 20 kPa. This is due to the components of the AFS reaching the extreme positions of their range of motion. It is also seen how the deflection response at higher angles of attack becomes lower (e.g. comparing the deflection curve at 0 deg vs. 10 deg) due to the external aerodynamic loading on the flap. Nevertheless, the magnitude of flap deflection due to aerodynamic loading is much lower than the flap deflection due to actuation pressure input.

The aerodynamic coefficients of the silicone AFS are measured for three characteristic pressure levels in the linear portion of the flap deflection range, namely 0, 10, and $20kPa$. The results for lift coefficient, and lift to drag ratio are shown in figure 6

The testing in the wind tunnel is performed at different Reynolds numbers (varying from 1 to 3 million), not with the purpose of studying the Reynolds sensitivity of the AFS, but to study the dependency of the deflection on the external aerodynamic loading of the flap, which within the context of this paper will be referred to as the *aerodynamic stiffness* of the system. Depending on the local pressure distribution on the AFS, the deflection obtained for different incoming wind speeds will differ when compared to the response in absence of wind. For the sake of conciseness, only measurements at a Reynolds number of 3 million are shown. (see figure 6). The measurements show that the impact of flow speed on the deflection of the system is negligible at low AoA (i.e. the deflection of the AFS is not strongly influenced by the external pressure field), where as this effect intensifies at high AoA. The AFS can thus be considered as aerodynamically stiff for the main portion of the linear range of the polars. The level of lift

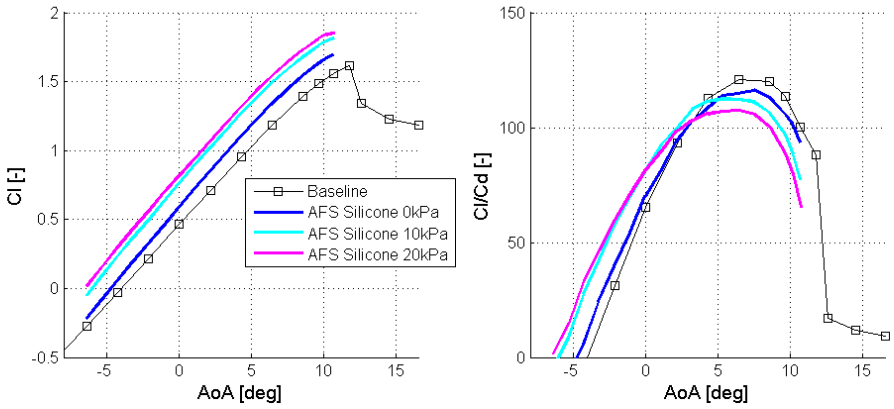

Figure 6: Aerodynamic coefficients of the silicone AFS in different actuation states. Left: lift coefficient, right: lift to drag ratio.

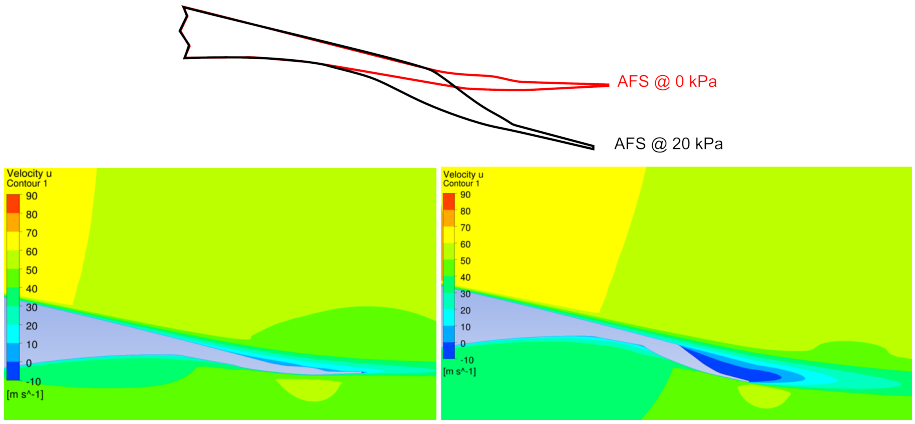

Figure 7: Detail of velocity field close to AFS in neutral (left) and active (right) position

variations obtained are in line with the expectations based on CFD simulations.

As previously discussed, one drawback of the very localized trailing edge deformation is the risk of suction side separation directly at the flap for high positive deflections (i.e. high pressure values). Such a separation region is shown in figure 7. Avoiding such separation regions is difficult with the type of flap considered here-in. An alternative would be a full morphing trailing edge as described e.g. in [14, 15].

4. Aeroelastic simulations

A set of aeroelastic calculations is run exemplarily on a SWT-4.0-130 turbine corresponding to a full set of Design Load Cases (DLCs) specified in IEC61400-1 [4]. This Design Load Basis (DLB) is used for the evaluation of the load potential for AFS applications. For this particular setup, the rotor was simulated with the active flaps in the outboard 16m of the blades. The added mass of the system (approx 40-50 kg per blade) has not been modelled, as this is below the typical mass tolerance levels for industrially manufactured blades and has an insignificant impact on eigenfrequencies. The feasibility for load reduction builds on top of the work of Barlas, et al. [2]. For the simulations, the aeroelastic solver BHawC (Siemens in-house aeroelastic solver [10, 11]) is used. The simulations are carried out for the two extreme flap positions as well as for a neutrally deflected flap, focusing on the effect on extreme loads. Fatigue loads have not been

Extreme loads				
Channel	DLC	Rel. diff. positive flap deflection [%]	DLC	Rel. diff. negative flap deflection [%]
Tower bottom bending fore-aft	DLC13_	4.2	DLC13_	-3.1
Tower bottom bending side-to-side	DLC62_	0.6	DLC62_	0.0
Tower top bending fore-aft	DLC24_	-2.5	DLC24_	-0.2
Tower top bending side-to-side	DLC24_	3.1	DLC24_	0.4
Shaft torsion	DLC13_	1.2	DLC13_	-0.5
Shaft thrust	DLC13_	3.2	DLC13_	-3.1
Hub Bending	DLC13_	2.4	DLC13_	-3.1
Blade root flap (min)	DLC13_	2.9	DLC13_	-2.7
Blade root flap (max)	DLC62_	-1.3	DLC62_	-0.1
Blade root edge (min)	DLC13_	-0.2	DLC24_	-1.0
Blade root edge (max)	DLC13_	-0.2	DLC13_	-2.0
Blade tip deflection	DLC13_	4.7	DLC13_	-6.1

Table 1: Relative load comparison between a flap with positive and negative deflection with respect to a flap with neutral deflection

under consideration within the scope of this paper, due to the low frequency foreseen ($< 1P$) for this type of AFS activation strategy. For a review of more generic types of smart rotor control the reader is referred to [3].

A summary of the relative load impact on some of the main components of the turbine is given in table 1. Furthermore, a relative comparison of mean blade flapwise loads at the blade root and at a midspan position at approx. 50% blade length, as well as the relative increase/decrease of blade deflection are shown in figures 8 and 9, respectively.

It can be seen that for most load channels, reductions in the order of magnitude of -3% are feasible for a full negative flap deflection. Most of these are related to DLC13 (extreme turbulence). In order to harvest these load reduction benefits, it is necessary to be able to distinguish between situations of high and low turbulence during turbine operation. Such a turbulence detection can be performed for example with help of the control algorithm described in [12] or in [13]. A load reduction of the order of mangnitude of 3% on main components would normally not be enough to argue a cost-out on a wind turbine nor a design change. On a new design however, a tower load reduction would can have a significant cost impact (for sections driven by extremes and not by fatigue). Extreme blade deflection reductions of the order of 5% are significant as they allow to design a lighter blade, which in turn results in lower hub fatigue and lower main bearing bending due to rotor overhang weight. The direct cost impact is not within the scope of this work, nor the impact on the levelized cost of energy (LCOE).

A blade deloading by means of negative flap deflection is not feasible during normal operation (DLC12) as this would lead to a loss in turbine power performance. On the other hand, an increase in blade loading (via positive flap deflections) would be beneficial for power production in the constant speed region prior to rated power (i.e. for wind speeds after the rated rotor speed is reached, but prior to reaching rated power). These wind speeds are normally characterized by low power coefficients due to the sub-optimal tip speed ratio. This can be compensated via higher blade loading. The AEP impact of such a strategy has not been within the scope of this work. The drawback of this increase in blade loading in the constant speed area is the higher blade deflection at critical wind speeds (see figure 9 in the range between $10 - 13m/s$). Nevertheless, this is not necessarily critical in case a turbulence detection can be implemented as previously mentioned.

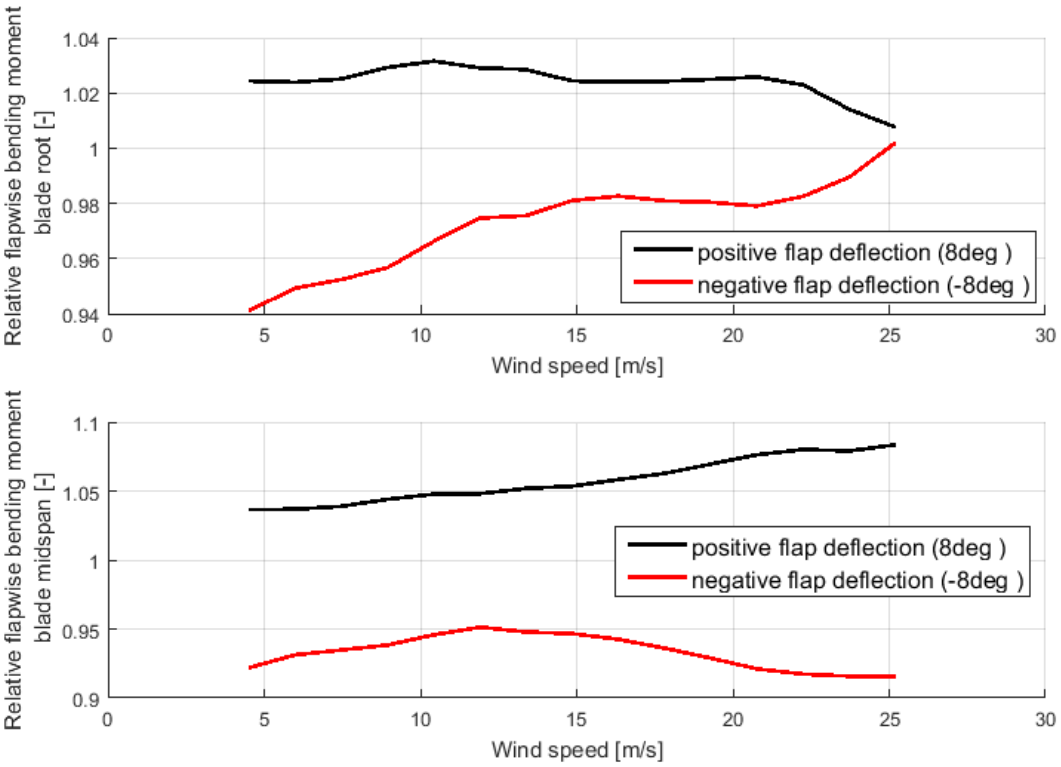

Figure 8: Relative blade flapwise bending moment comparison between a flap with positive and negative deflection with respect to a flap with neutral deflection. Upper: blade root, lower: 50% radial location.

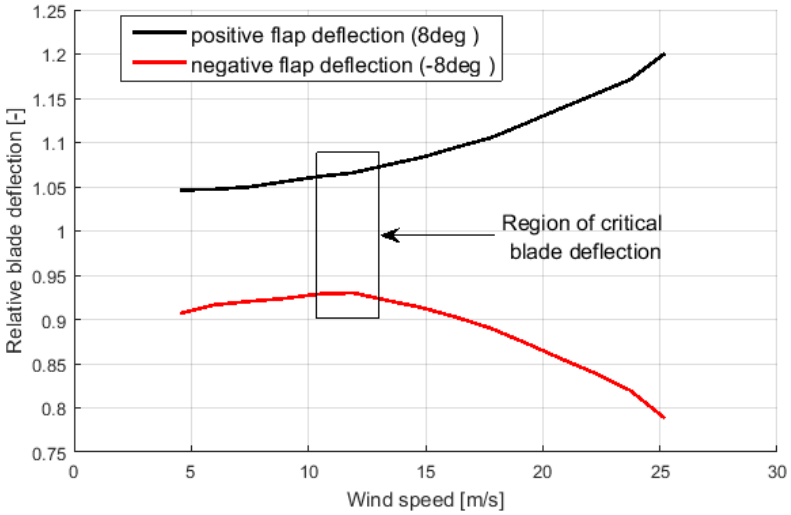

Figure 9: Relative blade flapwise deflection comparison between a flap with positive and negative deflection with respect to a flap with neutral deflection

5. Conclusions

A methodology for assessment of the aerodynamic performance of an airfoil retrofitted with an active flap system is shown and discussed. It is shown that for this type of airfoil-flap arrangement with a heavy loaded aft portion, a detailed description of the pressure distribution on the flap itself is compulsory due to the high levels of local curvature. For the estimation of pressure distribution, a hybrid description based on wind tunnel measurements and CFD simulations provides accurate results. Furthermore, the lift coefficient estimations are best obtained from wall pressure measurements.

An active flap system is designed and two pneumatically activated prototypes are manufactured with TPU and silicone. The elastic response of the TPU prototype is unsatisfactory. The silicone prototype is tested successfully and its aerodynamic system response is characterized as a function of input pressure.

The AFS system is simulated exemplarily on a SWT-4.0-130 turbine to assess the reduction potential for extreme loads. It is shown that with a combination of an AFS system with slow frequency actuation, load reduction in the order of magnitude of 3% are feasible for several main components.

Acknowledgments

The work has been funded by the Danish development and demonstration program EUDP under contract J.nr. 64015-0069 for the research project and research and development work Full scale demonstration of an active flap system for wind turbines.

References

[1] Induflap website. `http://www.induflap.dk/`
[2] Barlas, T 2016 Extreme load alleviation using industrial implementation of active trailing edge flaps in a full design load basis. The Science of Making Torque from Wind TORQUE2016. J. of. Phys. Conf. Series. 753 .
[3] Barlas, T K and van Kuik G A M. Review of state of the art in smart rotor control research for wind turbines. Progress in Aerospace Sciences - 2010 46 1, pp 1-27, 2010.
[4] International Standard IEC 61400-1:2005+AMD1:2010 Part 1: Design requirements. *Commission Electrotechnique Internationale*
[5] Energiteknologiske Udviklings- og Demonstrationsprogram. Danish Energy Agency. `https://ens.dk/ansvarsomraader/forskning-udvikling/eudp`
[6] Ansys CFX solver-theory guide, release 15, 2013.Ansys, Inc.
[7] Michelsen, J. A. Basis3D - a platform for development of multiblock PDE solvers. Technical Report AFM 92-05, Technical University of Denmark, 1992.
[8] Michelsen, J. A. Block structured multigrid solution of 2D and 3D elliptic PDEs. Technical Report AFM 94-06, Technical University of Denmark, 1994.
[9] Soerensen, N. N. General purpose flow solver applied to flow over hills. Technical Report Risoe-R- 827(EN), Risoe National Laboratory, 1995.
[10] Rubak, R., Petersen, J.T. Monopile as Part of Aeroelastic Wind Turbine Simulation Code. Proceedings of Copenhagen Offshore Wind. October, 2005. `http://wind.nrel.gov/public/SeaCon/Proceedings/Copenhagen.Offshore.Wind.2005/documents/papers/Design_calculations_and_risks/R.Rubak_Monopile_as_Part_of_Aeroelastic_WindTurbineSim.pdf`
[11] Skjoldan, P.F. Aeroelastic modal dynamics of wind turbines including anisotropic effects. PhD Thesis. DTU Risoe-PhD-66. 2011.
[12] Kanev, S. Extreme turbulence control for wind turbines. ECN-E–16-062. December 2016.
[13] Bischof, G., Rodenhausen, M. Intelligentes SektormanagementACS. Maximierung der Energieproduktion bei komplexen Windpark Konfigurationen. SpreeWindTage 2017.
[14] Madsen H A et al. Towards an industrial manufactured morphing trailing edge flap system for wind turbines, Proceedings of EWEC 2014, Barcelona, Spain 2014.
[15] Barlas, A. K., Akay, B. Optimization of morphing flaps based on fluid structure interaction modeling, 2018 Wind Energy Symposium, AIAA SciTech Forum, (AIAA 2018-0998)
[16] Menter, F., Zonal two equation Kappa-omega turbulence models for aerodynamic flows, 29th Fluid Dynamics Conference, July, 1993, (AIAA Journal 93-2906)